THE JOURNAL OF PHYSICAL CHEMISTRY LETTERS
A JOURNAL OF THE AMERICAN CHEMICAL SOCIETY

pubs.acs.org/JPCL

Letter

# Ultrafast Study of Excited State Dynamics of Amino Metal Halide Molecular Clusters

Heng Zhang, David C. Zeitz, and Jin Z. Zhang*

Cite This: J. Phys. Chem. Lett. 2023, 14, 8095−8099

Read Online

ACCESS | Metrics & More | Article Recommendations | Supporting Information

**ABSTRACT:** The excited state dynamics of ligand-passivated $PbBr_2$ molecular clusters (MCs) in solution have been investigated for the first time using femtosecond transient absorption spectroscopy. The results uncover a transient bleach (TB) feature peaked around 404 nm, matching the ground state electronic absorption band peaked at 404 nm. The TB recovery signal can be fitted with a triple exponential with fast (10 ps), medium (350 ps), and long (1.8 ns) time constants. The medium and long time constants are very similar to those observed in the time-resolved photoluminescence (TRPL) decay monitored at 412 nm. The TB fast component is attributed to vibrational relaxation in the excited electronic state while the medium component with dominant amplitude is attributed to recombination between the relaxed electron and hole. The small amplitude slow component is assigned to electrons in a relatively long-lived excited electronic state, e.g., triplet state, or shallow trap state due to defects. This study provides new insights into the excited state dynamics of metal halide MCs.

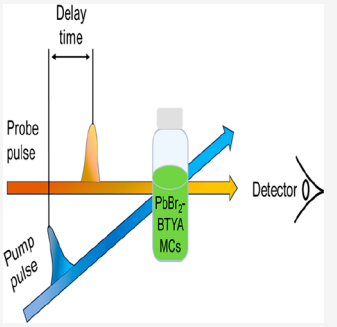




Recently, metal halide molecular clusters (MCs) have been subject to increasing interest due to their unique characteristics such as much smaller size and larger surface-to-volume (S/V) ratio compared to typical metal halide perovskite quantum dots (PQDs).[1−3] Their extremely small size results in stronger quantum-confined and bluer optical absorption and emission than PQDs.[4−10] In addition, they are potential intermediates to larger perovskite structures including PQDs and can be used to study the growth mechanisms of larger structures.[2,3,11]

Ligand-passivated $PbBr_2$ MCs exhibit first excitonic absorption and emission band peaked around 402 and 410 nm, respectively, which are bluer than both corresponding PQDs and perovskite magic-sized clusters (PMSCs).[2,3,8] Unlike their larger perovskite counterparts, the key difference among them is that metal halide MCs lack the A component that is present in PQDs and PMSCs with $ABX_3$ composition, as demonstrated by past work from our lab.[2] Also, further study showed that metal halide MCs can be generated alongside PQDs and PMSCs even when the A component is present.[12] More recent structural studies incorporating Raman, XRD, and TEM suggest that $PbBr_2$-BTYA MCs consist of a possible layered structure where the layers are composed of tilted, corner-sharing $[PbBr_6]^{4-}$ octahedra with a particle size of 2.0 ± 0.4 nm.[8] Although past work has shed insights into metal halide MCs' optical and structural properties, the excited state dynamics of the ligand-passivated $PbBr_2$ MCs that are relevant to many potential optoelectronic applications have not been studied yet.

In this work, femtosecond laser transient absorption spectroscopy was used to probe the excited state dynamics of ligand-passivated $PbBr_2$ MCs in a transient absorption configuration. The results reveal a relatively short overall excited state lifetime on the order of 350 ps, which is consistent with the relatively low photoluminescence quantum yield (PLQY) of 4%. The radiative and nonradiative lifetimes extracted from the observed lifetime and PLQY indicate that exciton decay is dominated by a nonradiative pathway.

To acquire a transient absorption (TA) signal, an ideal sample should be clear or nearly transparent. Stable MCs can be synthesized only with amine ligands, but they tend to be opaque. To achieve this, the $PbBr_2$-BTYA MCs precursor was modified by adding an acidic ligand, namely valeric acid, which results in a clear MC solution.[12]

Figure 1 shows the absorption and PL spectra of clear $PbBr_2$-BTYA MCs in solution, where the first electronic absorption and emission bands appear at 404 and 412 nm, respectively. The addition of valeric acid results in a nominal peak position difference of 3 nm for the absorption and 1 nm for the PL when compared with the $PbBr_2$-BTYA MCs reported previously, attributed to a minor difference in particle size.[2,7] The change in precursor composition for the synthesis of clear $PbBr_2$-BTYA MCs allows us to generate a sample that is sufficiently transparent for the femtosecond TA study, as shown in the Figure 1 inset. In addition, the PL spectrum shows a full width at half-maximum (FWHM) of 10 nm,

Received: July 14, 2023
Accepted: August 30, 2023




https://doi.org/10.1021/acs.jpclett.3c01952
J. Phys. Chem. Lett. 2023, 14, 8095−8099

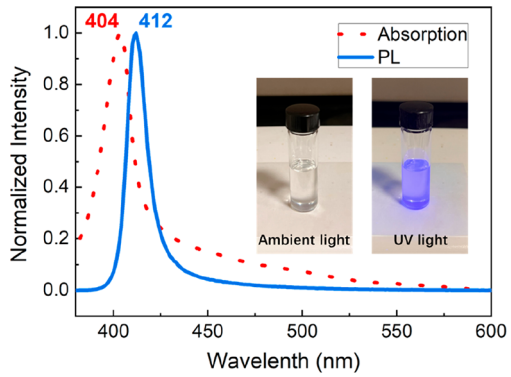


**Figure 1.** Optical properties of clear $PbBr_2$-BTYA MCs in solution. UV−vis absorption spectrum (red) and PL spectrum (blue) of clear $PbBr_2$-BTYA MCs in the solution state. Inset: images of clear MCs in solution state under ambient light and 365 nm UV light.

indicative of the narrow size distribution of this MC species.[2,6,7,12,13] Moreover, the Stokes shift observed between absorption and PL emission is only 8 nm, and there is no PL from trap states observed.

To determine the exciton dynamics of $PbBr_2$-BTYA MCs, femtosecond TA of colloidal $PbBr_2$-BTYA was measured in a pump−probe laser configuration. The TB spectra were collected with a pump wavelength of 370 nm, at a low pump power of 0.1 $\mu$J/pulse and probed by white light in the 350−550 nm region. Figure 2 shows TB spectra across the probe wavelength region of 390−440 nm from −1 to 100 ps (Figure 2a), from −1 to 1000 ps (Figure 2b), and a kinetic trace extracted from the peak TB signal at 404 nm from −1 to 4000 ps (Figure 2c). Both the spectra in Figure 2a and the kinetic trace in Figure 2c were modified to remove a strong positive feature immediately preceding $t_0$. This feature is attributed to coherent interference artifact induced between the pump and probe pulse.[14−19] Importantly, the spike was also seen in the toluene blank, where no sample was present, as shown in Figure S1, confirming that the removed feature near $t_0$ does not have a contribution from the sample itself. In Figure 2a, the TB signal first decreases to a minimum, limited by the laser pulse width, and then gradually recovers to zero. The TB band shows a maximum signal around 404 nm, which matches the first electronic absorption band peak at 404 nm.

In Figure 2b, the contour plot shows the 2D evolution of the TB signal in terms of both the delay time and wavelength. Consistent with Figure 2a, the strongest TB signal appears around 404 nm, and recovery to baseline persists over the probe range. The aforementioned coherent pump−probe interference is also shown here as a positive feature (red and green region) just before $t_0$ across the range of probed wavelength.[20,21]

Figure 2c is a TB decay profile at 404 nm plotted from −1 to 4000 ps with the associated fitting from 0 to 4000 ps shown in the inset. The TB recovery for pump power of 0.1 $\mu$J/pulse is well fitted with a triple-exponential function with time constants of 10 ps, 350 ps, and 1.8 ns. Similar TB profiles were measured with other excitation wavelengths of 360 and 380 nm, indicating that the dynamics are not dependent on excitation (pump) wavelength.[20]

To determine the possible power dependence of the excited state dynamics, we measured TB results with different pump powers. Figure 3 shows the TB profiles of $PbBr_2$-BTYA MCs probed at 404 nm over a range of pump powers. The artifact

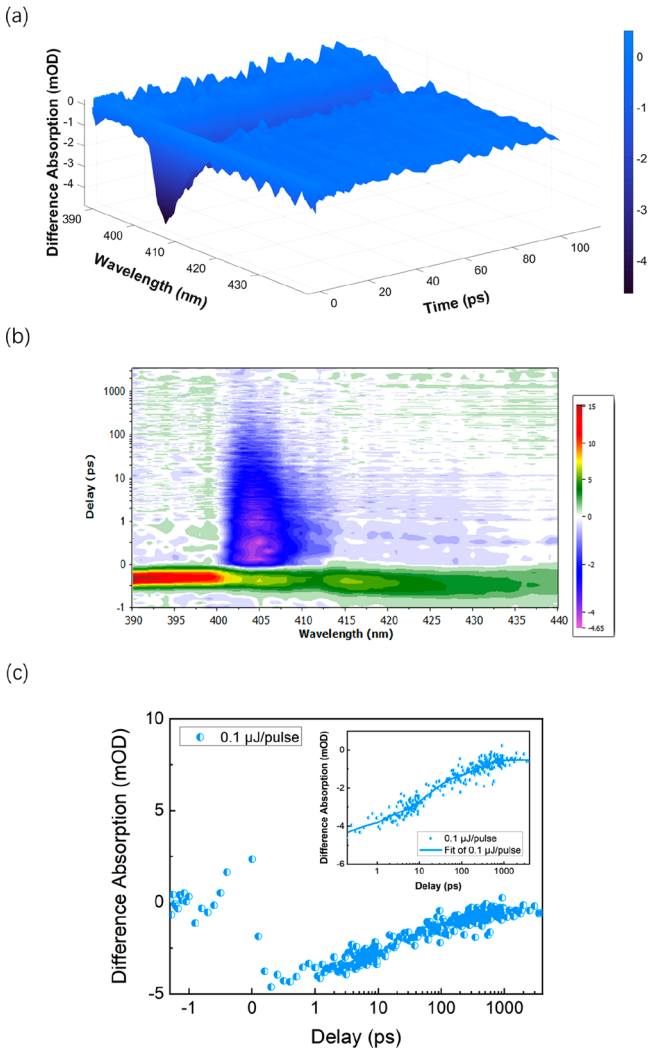


**Figure 2.** Transient bleach spectra of $PbBr_2$-BTYA MCs with excitation (pump) wavelength at 370 nm and probe wavelength in 390−440 nm region and pump power at 0.1 $\mu$J/pulse. (a) 3D plot on the −1 to 100 ps time scale. (b) 2D plot over −1 to 4000 ps time scale. (c) TB profile and associated fitting for TB profile at 404 nm in −1 to 4000 ps.

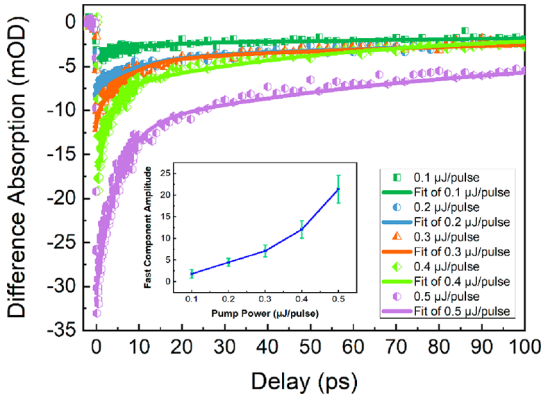


**Figure 3.** Transient bleach profile of $PbBr_2$-BTYA MCs under the pump powers at 0.1, 0.2, 0.3, 0.4, and 0.5 $\mu$J/pulse probed at 404 nm and excited at 370 nm. Inset: the power dependence of the fast component amplitude shows a linear process under low pump powers and a nonlinear process under high pump powers.



https://doi.org/10.1021/acs.jpclett.3c01952
J. Phys. Chem. Lett. 2023, 14, 8095−8099

spike near $t_0$ not reflecting a true decay feature was removed for ease of visualization of the data. The TB profiles show that the peak amplitude near $t_0$ increases with rising pump powers. The amplitude of the fast component increases linearly in the low power region (0.1−0.3 $\mu$J/pulse) but more than linearly under high pump powers (0.4−0.5 $\mu$J/pulse). However, because the amplitude becomes very small at low powers, it is not determined if the fast time constant has a real pump power dependence, although based on both the time constants and amplitudes, there appears to be a transition from linear regime under low pump powers to the nonlinear regime under high pump powers. Usually, a shorter lifetime is expected for higher power when nonlinear effects, such as exciton−exciton annihilation or Auger recombination, are involved.[20−24] The fitting parameters including amplitudes and time constants under five pump powers corresponding to Figure 3 are summarized in Tables S1 and S2. To better assess the linear and nonlinear regions, the fast component time constants were held constant at 10 ps, as shown in Table S1. In this way, it was determined that the amplitudes transition from a linear to a more than linear increase at high pump powers. In Table S2, this distinction between linear and nonlinear regions is supported by allowing the fast component to vary during fitting, the result of which shows a decreasing trend in the fast component time constants and a corresponding increase in amplitude transitioning from linear at low pump powers to more than linear at high pump powers. Both the 350 and 1800 ps decay time constants for medium and slow components were also held constant for all the fits based on the fitting result from TRPL due to the greatly improved signal-to-noise ratio and will be discussed later. To avoid possible nonlinear effects, we focus our discussion on the low pump powers data that are in the linear regime determined by the fast component amplitude and time constants.

Figure 4 shows the TRPL profile of the $PbBr_2$-BTYA MCs measured at 412 nm following excitation at 370 nm. The

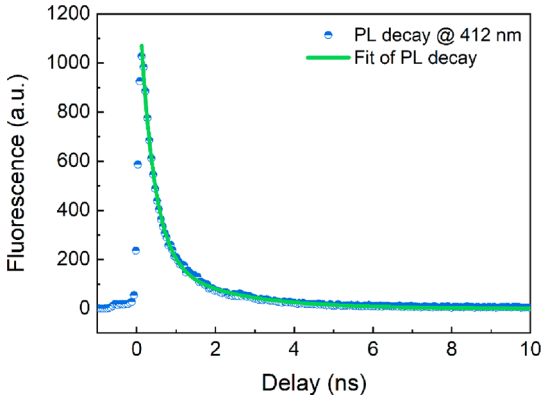


**Figure 4.** Time-resolved photoluminescence profile of $PbBr_2$-BTYA MCs monitored at 412 nm following excitation at 370 nm based on time-correlated single photon counting (TCSPC) measurements.

selection of excitation bluer than the absorption peak at 404 nm allows better separation of the PL emission from the excitation light that can interfere with the TRPL measurement. The TRPL profile can be fitted with two time constants of 350 ps and 1.8 ns with an error of less than 0.2%, which are used for the medium and long time constants of the TB results. Therefore, we suggest that the 350 ps component in TRPL and the 350 ps component in TB correspond to the same dynamic process, while similarly, the 1.8 ns component observed in both TRPL and TB is due to the same dynamic process.

To help gain deeper insight into exciton decay dynamics, the PLQY was measured using quinine sulfate as a reference and used along with the TB results to extract the radiative and nonradiative lifetimes. Figure 5 shows the fitted slopes

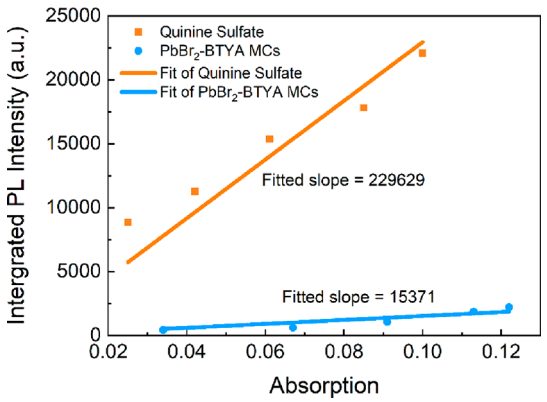


**Figure 5.** Linear correlation between integrated PL intensity versus absorption of quinine sulfate (orange) and $PbBr_2$-BTYA MCs (blue).

collected from both quinine sulfate and $PbBr_2$-BTYA MCs. The absorption of both samples was measured in the range of 0.02−0.1 optical density (OD) to facilitate a linear relationship between the integrated PL intensity and absorption. The PLQY of $PbBr_2$-BTYA MCs was calculated as 4%, and after combining the PLQY result with the lifetime of the dominant component of 350 ps, which we consider as the observed excited state lifetime $\tau_{obs}$, the radiative and nonradiative lifetimes were calculated based on eqs 1 and 2. The radiative lifetime is calculated as ∼9 ns, 24 times longer than the nonradiative lifetime of ∼365 ps, indicating that the dynamics are dominated by nonradiative decays.[25,26]

$$\frac{1}{\tau_{obs}} = \frac{1}{\tau_r} + \frac{1}{\tau_{nr}} \quad (1)$$

$$\phi_{PL} = \frac{\tau_{obs}}{\tau_\gamma} \quad (2)$$

Figure 6 illustrates the key dynamic processes in photoexcited $PbBr_2$-BTYA MCs that we proposed based on the spectroscopy and dynamics results. This model only illustrates the exciton dynamics under low pump powers, where there are no nonlinear dynamic processes that tend to occur under high pump powers, such as two-photon decays, exciton−exciton annihilation, and Auger recombination, which often complicate data analysis. Under low pump powers, upon photoexcitation, an electron is generated in the excited electronic state and a hole in the ground state, forming an exciton.[27,28] If possessing excess kinetic energy, the electron will relax to the bottom of the excited electronic state through vibrational relaxation via electron−phonon coupling. The relaxed electron can recombine radiatively, resulting in PL, or nonradiatively with the hole in the ground electronic state, resulting in a medium decay lifetime (∼350 ps) in TB which corresponds to a fast component (∼350 ps) in TRPL.[28] The small-amplitude slow component (1.8 ns) observed in both TB and TRPL is tentatively attributed to a relatively long-lived triplet or trap state that is coupled to the first excited electronic state responsible for the primary dynamics observed (dominant 350


https://doi.org/10.1021/acs.jpclett.3c01952
J. Phys. Chem. Lett. 2023, 14, 8095−8099

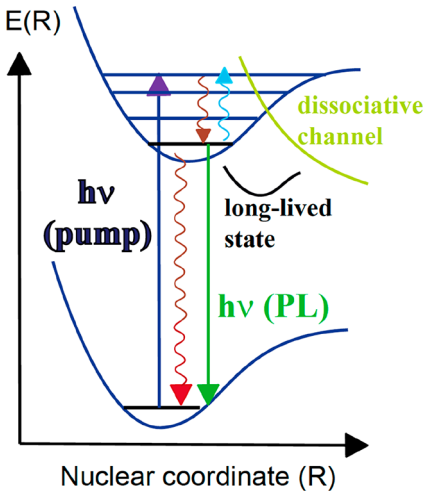


**Figure 6.** A proposed model for key dynamic processes in $PbBr_2$-BTYA MCs, including vibrational relaxation in the excited electronic state, recombination of relaxed electron and hole, a dissociative excited electronic state that leads to the overall short excited state lifetime, and a long-lived (>1 ns) triplet state or trap state that is coupled to the excited electronic state responsible for the primary dynamics observed including the PL and TRPL results.

ps decay with large amplitude). The dynamic signal observed is always a sum of the TA signal from the excited electronic state and the TB signal from the ground electronic state. What is observed depends on the relative intensity of the TA versus TB signals at a specific probe wavelength and at a specific time during the dynamic process. At the 404 nm probe wavelength, TB is dominant and was used by us to analyze the dynamics. Because the signal we measured involves both TA and TB with opposite signs, the amplitude and lifetime of the signal measured may have complex dependence on pump powers, however, the TB is dominating according to the transient absorption spectra shown in Figure S2. Thus, we should use both the amplitude and lifetime to analyze possible power dependence, such as linear versus nonlinear effects.

The triple-exponential decay of the TB signal indicates that the overall dynamics process is not a simple sequential or parallel process but involves energy transfer in the reverse direction, noted in Figure 6 as an upward curved arrow.[21,27] This back energy transfer process is usually expected to be much slower than the forward process.[27] Due to the limited dynamics data available such as all relevant time or rate constants, at present it is not possible to do meaningful kinetic modeling of the overall dynamics of the MCs studied. Instead, based on our previous kinetic modeling of PQDs,[20,27] we suggest that a likely reverse process is a back energy transfer from vibrationally relaxed states to hot states in the excited electronic state, which could result in the multiple exponential features observed. Overall, we attribute the short decay of 10 ps to vibrational relaxation in the first excited electronic state, the medium 350 ps decay to the recombination of the relaxed electron with the hole, and the long 1.8 ns decay to a relatively long-lived electronic state, which is coupled to the first excited electronic state and mediates its dynamics. The relatively narrow absorption band and small Stokes shift between the absorption and PL bands indicate a flat potential energy surface (PES) for the excited electronic state. The dominant nonradiative decay of the first excited electronic state could be due to strong coupling to a dissociative excited electronic state. On the other hand, the moderate lifetime of the first excited electronic state observed (dominated by the 350 ps component) suggests that this state is bound and not directly dissociative in itself.

However, if the MCs are more solid-like, an explanation of the dynamics using an electronic band structure would be more appropriate.[28] In this case, the 10 ps fast decay component may be attributed to the trapping of the charge carriers (electron or hole) into shallow trap states or self-trapped excisions (STE), while the 350 ps medium component is attributed to the recombination of trapped electron and hole following trapping. The 1.8 ns slow decay would be likely due to some long-lived deep trap states that are coupled to and mediate the dynamics of the shallow trap states. Similar to the above analysis, a reverse process is required to account for the multiple exponential decays observed, and we suggest detrapping from the shallow trap states to the conduction band (CB) as the reverse process. If this explanation is correct, the narrow absorption band and small Stokes shift between the absorption and PL bands would suggest that the trap states are shallow or near the band edge, about 60 meV below the CB edge. Also, the relatively low PLQY of 4% indicates the trapped carriers or trapped excitons, similar to self-trapped excitons, which decay primarily nonradiatively and are usually attributed to deep trap states due to defects.[29,30]

In summary, the excited state dynamics of $PbBr_2$ MCs passivated with butylamine and valeric acid were studied using femtosecond TA spectroscopy. A TB profile peaked at 404 nm shows a recovery that can be fitted with a triple exponential withthe fast (10 ps), medium (350 ps), and slow (1.8 ns) components. These decay components are attributed to vibrational relaxation within the first excited electronic state, relaxed electron−hole recombination coupled to a dissociative electronic state, and another long-lived excited electronic state. A PLQY of 4% is consistent with the overall moderately long excited state lifetime of these metal halide MCs, which is revealed for the first time using ultrafast laser spectroscopy. The results are important for gaining a deeper understanding of the photophysics of metal halide clusters and related metal halide perovskite clusters.

## ■ ASSOCIATED CONTENT

### Supporting Information

The Supporting Information is available free of charge at https://pubs.acs.org/doi/10.1021/acs.jpclett.3c01952.

Details of materials and synthesis, spectroscopic measurements (UV−vis absorption, photoluminescence spectra), ultrafast fs laser TA measurements, TA and TB spectra and detailed parameters of the TB and TRPL fitting results (PDF)

## ■ AUTHOR INFORMATION

### Corresponding Author

**Jin Z. Zhang** − *Department of Chemistry and Biochemistry, University of California, Santa Cruz, Santa Cruz, California 95064, United States;* orcid.org/0000-0003-3437-912X; Email: zhang@ucsc.edu

### Authors

**Heng Zhang** − *Department of Chemistry and Biochemistry, University of California, Santa Cruz, Santa Cruz, California 95064, United States;* orcid.org/0000-0001-8521-5403



https://doi.org/10.1021/acs.jpclett.3c01952
J. Phys. Chem. Lett. 2023, 14, 8095−8099

**David C. Zeitz** − *Department of Chemistry and Biochemistry, University of California, Santa Cruz, Santa Cruz, California 95064, United States*

Complete contact information is available at: https://pubs.acs.org/10.1021/acs.jpclett.3c01952

### Notes

The authors declare no competing financial interest.

## ■ ACKNOWLEDGMENTS

We acknowledge financial support from National Science Foundation (CHE-2203633). We thank Allison Win and Celia Todd for helpful discussions and assistance in some sample preparation.

## ■ REFERENCES

(1) Zhou, C.; Lin, H.; Worku, M.; Neu, J.; Zhou, Y.; Tian, Y.; Lee, S.; Djurovich, P.; Siegrist, T.; Ma, B. Blue Emitting Single Crystalline Assembly of Metal Halide Clusters. *J. Am. Chem. Soc.* **2018**, *140* (41), 13181−13184.

(2) Vickers, E. T.; Chen, Z.; Cherrette, V.; Smart, T.; Zhang, P.; Ping, Y.; Zhang, J. Z. Interplay between Perovskite Magic-Sized Clusters and Amino Lead Halide Molecular Clusters. *Research* **2021**, *2021*, 1−7.

(3) Liu, L.; Pan, K.; Xu, K.; Peng, X.; Zhang, J. Z. Synthesis and Optical Properties of $Mn^{2+}$-Doped Amino Lead Halide Molecular Clusters Assisted by Chloride Ion. *J. Phys. Chem. Lett.* **2021**, *12* (31), 7497−7503.

(4) Liu, L.; Xu, K.; Vickers, E. T.; Allen, A.; Li, X.; Peng, L.; Zhang, J. Z. Varying the Concentration of Organic Acid and Amine Ligands Allows Tuning between Quantum Dots and Magic-Sized Clusters of $CH_3NH_3PbBr_3$ Perovskite: Implications for Photonics and Energy Conversion. *Acs Appl. Nano Mater.* **2020**, *3* (12), 12379−12387.

(5) Guarino-Hotz, M.; Barnett, J. L.; Pham, L. B.; Win, A. A.; Cherrette, V. L.; Zhang, J. Z. Tuning between Methylammonium Lead Bromide Perovskite Magic-Sized Clusters and Quantum Dots through Ligand Assisted Reprecipitation at Elevated Temperatures. *J. Phys. Chem. C* **2022**, *126* (32), 13854−13862.

(6) Xu, K.; Allen, A. C.; Luo, B.; Vickers, E. T.; Wang, Q.; Hollingsworth, W. R.; Ayzner, A. L.; Li, X.; Zhang, J. Z. Tuning from Quantum Dots to Magic Sized Clusters of $CsPbBr_3$ Using Novel Planar Ligands Based on the Trivalent Nitrate Coordination Complex. *J. Phys. Chem. Lett.* **2019**, *10* (15), 4409−4416.

(7) Zhang, H.; Vickers, E. T.; Erickson, S.; Guarino-Hotz, M.; Barnett, J. L.; Ghosh, S.; Zhang, J. Z. Synthesis and Properties of Stable Amino Metal Halide Molecular Clusters in the Solid State. *J. Phys. Chem. Lett.* **2022**, *13* (45), 10543−10549.

(8) Xu, K.; Vickers, E. T.; Luo, B.; Wang, Q.; Allen, A. C.; Wang, H.; Cherrette, V.; Li, X.; Zhang, J. Z. Room Temperature Synthesis of Cesium Lead Bromide Perovskite Magic Sized Clusters with Controlled Ratio of Carboxylic Acid and Benzylamine Capping Ligands. *Sol. Energy Mater. Sol. Cells* **2020**, *208*, 110341.

(9) Vickers, E. T.; Xu, K.; Dreskin, B. W.; Graham, T. A.; Li, X.; Zhang, J. Z. Ligand Dependent Growth and Optical Properties of Hybrid Organo-Metal Halide Perovskite Magic Sized Clusters. *J. Phys. Chem. C* **2019**, *123* (30), 18746−18752.

(10) Guarino-Hotz, M.; Barnett, J. L.; Chou, K.-C.; Win, A. A.; Zhang, H.; Song, C.; Oliver, S. R. J.; Zhang, J. Z. Structural Study of Paraffin-Stabilized Methylammonium Lead Bromide Magic-Sized Clusters. *J. Phys. Chem. C* **2023**, *127* (6), 3367−3376.

(11) Liu, L.; Pan, K.; Xu, K.; Zhang, J. Z. Impact of Molecular Ligands in the Synthesis and Transformation between Metal Halide Perovskite Quantum Dots and Magic Sized Clusters. *ACS Phys. Chem. Au* **2022**, *2* (3), 156−170.

(12) Win, A.; Chou, K. C.; Zeitz, D. C.; Todd, C.; Zhang, J. Z. Origin of the near 400 nm Absorption and Emission Band in the Synthesis of Cesium Lead Bromide Nanostructures: Metal Halide Molecular Clusters Rather Than Perovskite Magic-Sized Clusters. *J. Phys. Chem. Lett.* **2023**, *14* (1), 116−121.

(13) Xu, K.; Vickers, E. T.; Luo, B.; Allen, A. C.; Chen, E.; Roseman, G.; Wang, Q.; Kliger, D. S.; Millhauser, G. L.; Yang, W.; Li, X.; Zhang, J. Z. First Synthesis of Mn-Doped Cesium Lead Bromide Perovskite Magic Sized Clusters at Room Temperature. *J. Phys. Chem. Lett.* **2020**, *11* (3), 1162−1169.

(14) Luo, C.-W.; Wang, Y.; Chen, F.; Shih, H. A.; Kobayashi, T. Eliminate Coherence Spike in Reflection-Type Pump-Probe Measurements. *Opt. Express* **2009**, *17* (14), 11321−11321.

(15) Borri, P.; Romstad, F.; Langbein, W.; Kelly, A.; Mork, J.; Hvam, J. Separation of Coherent and Incoherent Nonlinearities in a Heterodyne Pump-Probe Experiment. *Opt. Express* **2000**, *7* (3), 107−107.

(16) Vardeny, Z.; Tauc, J. Picosecond Coherence Coupling in the Pump and Probe Technique. *Opt. Commun.* **1981**, *39* (6), 396−400.

(17) Palfrey, S. L.; Heinz, T. F. Coherent Interactions in Pump-Probe Absorption Measurements: The Effect of Phase Gratings. *J. Opt. Soc. Am. B* **1985**, *2* (4), 674−674.

(18) Cundiff, S. T. Coherent Spectroscopy of Semiconductors. *Opt. Express* **2008**, *16* (7), 4639.

(19) Liu, H.; Zhang, H.; Si, J.; Yan, L.; Chen, F.; Hou, X. Elimination of the Coherent Artifact in a Pump-Probe Experiment by Directly Detecting the Background-Free Diffraction Signal. *Chin. Phys. Lett.* **2011**, *28* (8), 086602−086602.

(20) Wheeler, D. A.; Huang, J.-A.; Newhouse, R.; Zhang, W.-F.; Lee, S.-T.; Zhang, J. Z. Ultrafast Exciton Dynamics in Silicon Nanowires. *J. Phys. Chem. Lett.* **2012**, *3* (6), 766−771.

(21) Pu, Y.-C.; Kibria, M. G.; Mi, Z.; Zhang, J. Z. Ultrafast Exciton Dynamics in InGaN/GaN and $Rh/Cr_2O_3$ Nanoparticle-Decorated InGaN/GaN Nanowires. *J. Phys. Chem. Lett.* **2015**, *6* (13), 2649−2656.

(22) Burda, C.; Link, S.; Mohamed, M. B.; El-Sayed, M. The Pump Power Dependence of the Femtosecond Relaxation of CdSe Nanoparticles Observed in the Spectral Range from Visible to Infrared. *J. Chem. Phys.* **2002**, *116* (9), 3828−3833.

(23) Zheng, J. P.; Kwok, H. S. Exciton and Biexciton Recombination in Semiconductor Nanocrystals. *Appl. Phys. Lett.* **1994**, *65* (9), 1151−1153.

(24) Xu, X.; Zhao, Y.; Sie, E. J.; Lu, Y.; Liu, B.; Ekahana, S. A.; Ju, X.; Jiang, Q.; Wang, J.; Sun, H.; Sum, T. C.; Huan, C. H. A.; Feng, Y. P.; Xiong, Q. Dynamics of Bound Exciton Complexes in CdS Nanobelts. *ACS Nano* **2011**, *5* (5), 3660−3669.

(25) Brelle, M.; Torres-Martinez, C.; McNulty, J.; Mehra, R.; Zhang, J. Synthesis and Characterization of Cu x S Nanoparticles. Nature of the Infrared Band and Charge-Carrier Dynamics. *Pure Appl. Chem.* **2000**, *72*, 101−117.

(26) Wu, F.; Zhang, J. Z.; Kho, R.; Mehra, R. K. Radiative and Nonradiative Lifetimes of Band Edge States and Deep Trap States of CdS Nanoparticles Determined by Time-Correlated Single Photon Counting. *Chem. Phys. Lett.* **2000**, *330* (3), 237−242.

(27) Naghadeh, S. B.; Luo, B.; Pu, Y.-C.; Schwartz, Z.; Hollingsworth, W. R.; Lindley, S. A.; Brewer, A. S.; Ayzner, A. L.; Zhang, J. Z. Size Dependence of Charge Carrier Dynamics in Organometal Halide Perovskite Nanocrystals: Deciphering Radiative Versus Nonradiative Components. *J. Phys. Chem. C* **2019**, *123* (7), 4610−4619.

(28) Wheeler, D. A.; Zhang, J. Z. Exciton Dynamics in Semiconductor Nanocrystals. *Adv. Mater.* **2013**, *25* (21), 2878−2896.

(29) Meng, J.; Lan, Z.; Abdellah, M.; Yang, B.; Mossin, S.; Liang, M.; Naumova, M.; Shi, Q.; Sol Gutiérrez, Á.; Liu, Y.; Lin, W.-H.; Castelli, I. E.; Canton, S. E.; Pullerits, T.; Zheng, K. Modulating Charge-Carrier Dynamics in Mn-Doped All-Inorganic Halide Perovskite Quantum Dots through the Doping-Induced Deep Trap States. *J. Phys. Chem. Lett.* **2020**, *11* (9), 3705−3711.

(30) Ye, J.; Byranvand, M. M.; Martínez, C. O.; Hoye, R. L. Z.; Saliba, M.; Polavarapu, L. Defect Passivation in Lead-Halide Perovskite Nanocrystals and Thin Films: Toward Efficient LEDs and Solar Cells. *Angew. Chem., Int. Ed.* **2021**, *60* (40), 21636−21660.